Frontiers of Environmental Science & Engineering
2025, 19(6): 77 https://doi.org/10.1007/s11783-025-1997-4

RESEARCH ARTICLE

Combustion-related activities dominate atmospheric ammonia in the Pearl River Delta region, China

Mengzhi He[1], Junwen Liu ✉ [1], Chenglei Pei[2], Fan Jiang[1], Zixi Chen[1], Xueqin Zheng[1], Xiaoxiao Yang[1], Guanghui Li[1], Zheng Zong[3], Fang Cao[4], Yanlin Zhang[4], Chongguo Tian[5]

1. College of Environment and Climate, Institute for Environmental and Climate Research, Jinan University, Guangzhou 511443, China
2. Guangzhou Sub-branch of Guangdong Ecological and Environmental Monitoring Center, Guangzhou 510006, China
3. Environment Research Institute, Shandong University, Qingdao 266237, China
4. School of Ecology and Applied Meteorology, Nanjing University of Information Science and Technology, Nanjing 210044, China
5. CAS Key Laboratory of Coastal Environmental Processes and Ecological Remediation, Yantai Institute of Coastal Zone Research (YIC), Chinese Academy of Sciences (CAS), Yantai 264003, China

HIGHLIGHTS

- The NH_4^+ concentrations showed no significant differences at different altitudes.
- The $\delta^{15}N\text{-}NH_4^+$ values decreased with increasing altitude in urban areas.
- Combustion source was the largest emitter for NH_3 in the PRD region.
- The contributions of different sources to NH_3 vary with height.

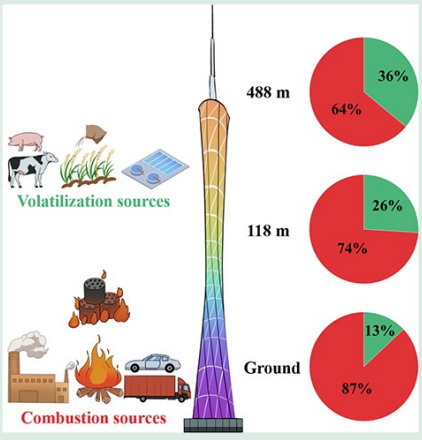

ABSTRACT: Ammonia (NH_3) is a key precursor of fine particulate matter ($PM_{2.5}$) in the air; however, its emission sources at different heights remain poorly understood in the Pearl River Delta (PRD) region of China. In this study, we simultaneously collected $PM_{2.5}$ samples at three atmospheric heights (ground, 118 m, and 488 m) based on the atmospheric observatories of Canton Tower, the tallest structure in the PRD region. Our results showed that the average NH_4^+ concentrations were 2.7 ± 1.4, 3.0 ± 1.8, and 2.6 ± 1.7 μg/m^3 at the ground site, 118 m, and 488 m during the sampling campaign, with no significant difference ($p > 0.05$) among the three heights. However, the stable nitrogen isotope composition values in NH_4^+ ($\delta^{15}N\text{-}NH_4^+$) displayed a significant correlation with height ($p < 0.05$). We further calculated the initial $\delta^{15}N\text{-}NH_3$ values and performed source apportionments using the Bayesian Isotope Mixture Model. The results indicated that the mean contributions of agriculture, waste, vehicle, biomass burning, NH_3 slip, and coal combustion were 9.9% ± 4.4%, 8.3% ± 5.5%, 29% ± 8.0%, 16% ± 2.2%, 25% ±

✉ Corresponding author. E-mail: liu.junwen@jnu.edu.cn
Article history: Received 12 December 2024, Revised 25 March 2025, Accepted 26 March 2025, Available online 15 April 2025

6.0%, and 12% ± 3.4%, respectively, at the ground site during the sampling campaign. By contrast, the contributions of sources at 488 m remained relatively stable due to the limited influence of local activities. Overall, our study highlights the dominant role of combustion sources in NH_3 emissions in the PRD region, with their contribution being highly dependent on atmospheric height.

KEYWORDS: Ammonia, Stable nitrogen isotope, Source apportionment, Canton Tower, PRD region

1 Introduction

As the most abundant alkaline gas in the atmosphere, ammonia (NH_3) can effectively react with acidic substances (e.g., SO_2 and NO_x) and transfer to ammonium aerosol (NH_4^+), which is a significant component of fine particulate matter ($PM_{2.5}$) with an aerodynamic diameter of less than 2.5 μm (Wei et al., 2023). On average, the mass contribution of NH_4^+ in $PM_{2.5}$ is approximately 5% globally (Weagle et al., 2018). Yet, this contribution would increase to 10%–20% during severe haze pollution events in regions with intensive anthropogenic activities, such as East Asia and South Asia (Nirmalkar et al., 2023; Wang et al., 2023a). To date, both field observations and simulation model studies have confirmed that reducing NH_3 emissions is a cost-effective strategy for the mitigation of $PM_{2.5}$ pollution in the world (Gu et al., 2021; Xu et al., 2022; Zheng et al., 2022; Vo and Christiansen, 2024).

Technology-based bottom-up emission inventories (EI) indicate that atmospheric NH_3 primarily originates from fertilizer application, livestock, waste, vehicle, coal combustion, and biomass burning. Agricultural sources, namely fertilizer application and livestock, are generally considered the largest emitter globally, contributing 83% (U.S.EPA, 2023), 93% (EEA, 2023), 83% (Li et al., 2021), and 81% (Sahoo et al., 2024) in the USA, Europe, China, and India, respectively. However, a large uncertainty exists in estimating NH_3 emissions based on EI methodology due to the highly variable emission factors of key sources. For instance, Farren et al. (2020) measured NH_3 emissions from 230000 passenger cars and found that current EI-derived NH_3 emissions are underestimated by a factor of 17. In addition, long-term global satellite observations have revealed that industry is a substantial source of atmospheric NH_3 and is underestimated by at least one order of magnitude by EI (Van Damme et al., 2018). Since the adopted emission factors and the associated activities of sources depend on the information obtained by researchers, EI-based NH_3 estimates for specific regions (e.g., China) often lack sufficient convergence (Li et al., 2017a; Li et al., 2021). This may lead to significant errors when formulating NH_3 reduction policies and assessing the impacts of NH_3 reductions on air quality using atmospheric chemical transportation models.

The stable nitrogen isotope composition ($\delta^{15}N$) is a reliable tool for source apportionment of atmospheric NH_3, as it provides distinct signatures of $\delta^{15}N$-NH_3 in key emission sources. For example, Pan et al. (2016) quantified the relative contributions of agricultural emission, NH_3 slip, and fossil fuel in atmospheric NH_3 in Beijing, China, finding that agricultural contributions accounted for 84% on clean days and 10% on hazy days. In Colorado's Front Range urban corridor, Felix et al. (2023) found that vehicle was the largest emitter (37%) of atmospheric NH_3, followed by biomass burning (34%), livestock (18%), and fertilizer (12%). Most $\delta^{15}N$-related studies focusing on the source apportionment of NH_3 or NH_4^+ have primarily examined the atmosphere near ground level (Xiao et al., 2020; Chang et al., 2021; Feng et al., 2022; Walters et al., 2022; Feng et al., 2023; Kawashima et al., 2023; Li et al., 2023; Zhang et al., 2023). However, knowledge of its vertical distribution remains poorly constrained due to the difficulties associated with sampling (Li et al., 2017b; Wu et al., 2019; Wu et al., 2024). For example, Wu et al. (2019) measured the concentration and $\delta^{15}N$ signatures of NH_4^+ in $PM_{2.5}$ samples collected at three atmospheric heights (8 m, 120 m, and 260 m) on a 325 m tower in Beijing, North China. Their results indicated that the relative contributions of emission sources to NH_4^+ were not uniform, with combustion sources playing a more significant role at the ground level compared to higher atmospheric altitudes. This finding was further corroborated by a recent study based on tower observations conducted at the same site (Wu et al., 2024). However, these studies were limited to North China and specific seasons, with the maximum sampling height restricted to 260 m. Such limitations hinder a comprehensive understanding of the sources of atmospheric NH_3 across different seasons, regions, and higher altitudes. Compared to the ground site, the

higher atmosphere is less affected by local sources, thus better representing the regional characteristics of the research area. In this study, year-long $PM_{2.5}$ samples were simultaneously collected from three different heights (ground, 118 m, 488 m) using atmospheric observatories at Canton Tower in Guangzhou, the largest city in South China. We also measured the $\delta^{15}N$ signatures of NH_4^+ and systematically investigated the vertical variations in the relative contributions of key NH_3 sources, which will significantly enhance our understanding of NH_3 sources and provide valuable insights for formulating effective emission reduction policies in this megacity.

2 Materials and methods

2.1 Aerosol sampling

The sampling campaign was conducted as part of the PRD region Aerosol Isotope Observation (PRDAIO) project (Chen et al., 2022; Jiang et al., 2022; 2023; Wang et al., 2023b). Three high-volume $PM_{2.5}$ samplers ($PM_{2.5}$-ASM-1, Guangzhou Mingye Environmental Protection Technology Co., Ltd., China) with a flow rate of 1 m^3/min were installed at three atmospheric observatories (ground, 118 m, and 488 m) at the Canton Tower in Guangzhou (113.3°E, 23.1°N), China. Guangzhou, the largest city in South China, is situated in the Pearl River Delta region (PRD) and is a highly urbanized metropolis with a population of approximately 18 million. The Canton Tower, the tallest structure in the PRD region, is located in downtown Guangzhou and is surrounded by dense traffic networks and residential areas. A total of more than 100 48-h $PM_{2.5}$ samples were simultaneously collected using quartz microfiber filters (0.052 m^2, Whatman, UK) at the three heights from October 2018 to August 2019.

2.2 Measurements of NH_4^+ concentration and stable nitrogen isotope

Before sampling, all quartz filters were heated in a muffle furnace at 450 °C for 6 h to eliminate potential impurities. After sampling, all filter samples were stored in a refrigerator at −20 °C until analysis. Quartz filters were treated with 20 mL of ultrapure water and sonicated for 40 min. Subsequently, the extracted solutions were filtered through 0.22 μm membranes, and the concentrations of NH_4^+ in the solutions were determined using an ion chromatograph (Dionex ICS-5000, Thermo Fisher Scientific Inc., USA). The mean instrumental detection limit (LOD) and measured precision were < 5 μg/L and ± 5%, respectively (Chen et al., 2022).

For the $\delta^{15}N$ measurements, the NH_4^+ was initially converted to nitrite (NO_2^-) using hypobromite (BrO^-) (AR, Sinopharm Chemical Reagent Co., Ltd, China), which was subsequently transformed into nitrous oxide (N_2O) using hydroxylamine (NH_2OH) (AR, Sinopharm Chemical Reagent Co., Ltd, China) under strongly acidic conditions. Finally, the isotopic analysis was conducted using an isotope ratio mass spectrometer (MAT253, Thermo Fisher Scientific, USA) (Liu et al., 2018). The $\delta^{15}N$-NH_4^+ values are reported relative to the standard (atmospheric N_2) and expressed in parts per thousand (‰) according to the following equation (Eq. (1)):

$$\delta^{15}N(‰) = [(^{15}N/^{14}N)_{sample} - (^{15}N/^{14}N)_{standard}]/(^{15}N/^{14}N)_{standard} \times 1000. \quad (1)$$

Each sample was calibrated using three international reference materials (IAEA-N1, USGS25, and USGS26), which have $\delta^{15}N$ values of 0.4‰, −30.4‰, and 53.7‰, respectively. The analytical precision for the $\delta^{15}N$-NH_4^+ measurements was better than 0.3 ‰ (Liu et al., 2014).

2.3 Calculation of the initial $\delta^{15}N$-NH_3

The initial $\delta^{15}N$-NH_3 can be calculated using the isotope mass balance model (Pan et al., 2016) as follows (Eq. (2)):

$$\delta^{15}N\text{-}NH_{3(gas)} = \delta^{15}N\text{-}NH^+_{4(aerosol)} - \varepsilon_{(NH_4^+\text{-}NH_3)} \times (1-f). \quad (2)$$

In the above equation, $\delta^{15}N$-$NH_{3(gas)}$ and $\delta^{15}N$-$NH_4^+{}_{(aerosol)}$ denote the $\delta^{15}N$ value of initial NH_3 and the measured $\delta^{15}N$ value of aerosol NH_4^+, respectively. The parameter f means the fraction of NH_3 converted into aerosol NH_4^+. Since NH_3 was not collected during the sampling campaign in this study, the f value was derived from a previous study that simultaneously measured the concentrations of NH_3 and NH_4^+ in the PRD region (Yue et al., 2015). ε is the nitrogen isotopic enrichment factor (Eq. (3)), which is a function of temperature (T, Kelvin) (Urey, 1947; Li et al., 2012; Kawashima and Ono, 2019; Walters et al., 2019):

$$\varepsilon_{(NH_4^+-NH_3)} = 12.4678 \times 1000/T - 7.6694. \quad (3)$$

2.4 Isotope mixing model

The Stable Isotope Analysis in R (SIAR) package was used to quantify the relative contributions of major sources to atmospheric NH_3 (Parnell et al., 2010). SIAR

integrates the isotopic signatures ($\delta^{15}N$) and associated uncertainties of potential sources, providing probabilistic estimates of their contributions. The initial $\delta^{15}N\text{-}NH_3$ in the atmosphere was treated as a mixture of multiple sources. The isotopic endmembers of key sources were parameterized using a prior distribution based on a newly established NH_3 source profile, incorporating both the mean and variance. The model applies Monte Carlo simulations to reconcile the initial $\delta^{15}N\text{-}NH_3$ value of the mixture with the distributions of potential source endmembers. Each stimulation iteration generated percentage data for source contribution estimates. Final results, derived from 10000 potential solutions, account for variability in isotopic measurements, fractionation processes, and uncertainty in source proportion estimation. This methodological approach enables detailed quantification of source apportionment and provides critical insights into dominant contributors under varying atmospheric conditions.

3 Results and discussion

3.1 Vertical profile of meteorological parameters and NH_4^+ concentration level

The meteorological parameters observed at the Canton Tower exhibit strong associations with altitude (Fig. 1). For example, the average temperature during the sampling campaign was 24.6 ± 5.1 °C at the ground site, while it decreased to 23.1 ± 4.8 °C at 118 m and 20.3 ± 4.5 °C at 488 m (Table S1). By contrast, wind speed exhibited a significant increasing trend with increasing height. During the entire observation period, the wind speeds at the ground site, 118 m, and 488 m were 0.63 ± 0.2, 2.2 ± 0.9, and 3.1 ± 1.2 m/s, respectively. Obviously, this vertical variation in meteorological parameters is beneficial for the transport of air pollutants from the ground to higher altitudes. Furthermore, the atmospheric environment at 488 m is more susceptible to the impacts of regional transportation due to its strongest wind speed among the three heights.

The average NH_4^+ concentrations at the ground site, 118 m, and 488 m were 2.7 ± 1.4, 3.0 ± 1.8, and 2.6 ± 1.7 μg/m^3, respectively. However, the differences in NH_4^+ concentrations among the three heights were not statistically significant ($p > 0.05$) (Fig. 1), suggesting that the NH_4^+ was uniformly mixed across the heights during the 48-h sampling period. We further investigated the correlation between NH_4^+ concentrations and meteorological parameters. The results showed that all NH_4^+ concentrations at all three heights were not significantly correlated with temperature or humidity ($p > 0.05$), with low R values (Figs. S1–S3). However, significant and negative correlations were observed between NH_4^+ concentrations and wind speed at 118 m and 488 m ($p < 0.05$) (Figs. S2 and S3), suggesting that NH_4^+ levels at higher altitudes are more influenced by regional transportation. By contrast, no significant correlation was found between NH_4^+ concentration and wind speed at the ground site ($p > 0.05$) (Fig. S1), reflecting the strong impact of local NH_3 emission on the ground NH_4^+ concentration. Overall, the average mass percentage of NH_4^+ in $PM_{2.5}$ in this study was approximately 6% and $PM_{2.5}$ concentrations at all heights showed a strong increase alongside rising NH_4^+ concentrations ($p < 0.001$), indicating that NH_4^+ is a key component regulating the $PM_{2.5}$ pollution in Guangzhou area.

3.2 Vertical profile of $\delta^{15}N\text{-}NH_4^+$ signature

Although NH_4^+ concentrations did not vary significantly across altitudes, we found that $\delta^{15}N\text{-}NH_4^+$ values at Canton Tower exhibited significant variation with heights ($p < 0.05$) (Fig. 1 and Table 1). The average $\delta^{15}N\text{-}NH_4^+$ values at the ground site, 118 m, and 488 m were 16‰ ± 5.2‰, 12‰ ± 3.8‰, and 7.4‰ ± 7.1‰, respectively. The observed $\delta^{15}N\text{-}NH_4^+$ values in this study displayed a decreasing trend as NH_4^+ concentrations increased, with a more pronounced negative correlation at higher altitudes (Fig. S1–S3), indicating that the increase in NH_4^+ concentration at high heights is associated with greater ^{15}N depletion. The $\delta^{15}N\text{-}NH_4^+$ values in this study were approximately 2 to 3 times higher than those observed in Beijing, North China, using a 325 m meteorological tower (Table S2). Given the substantial difference in $\delta^{15}N\text{-}NH_4^+$ values between the two cities, we inferred that NH_3 in Guangzhou may be more impacted by anthropogenic sources characterized by $\delta^{15}N$ enrichment, resulting in higher $\delta^{15}N$ compared to Beijing. Additionally, we found that the $\delta^{15}N\text{-}NH_4^+$ values in both Guangzhou and Beijing decreased with increasing height (Table S2) (Wu et al., 2019; Wu et al., 2024), suggesting that the upper atmosphere is more susceptible to low $\delta^{15}N\text{-}NH_3$ sources such as livestock and fertilizer application in the adjacent areas.

3.3 $\delta^{15}N\text{-}NH_3$ endmembers of sources

The current bottom-up emission inventory indicates that nearly all NH_3 in the PRD region comes from the

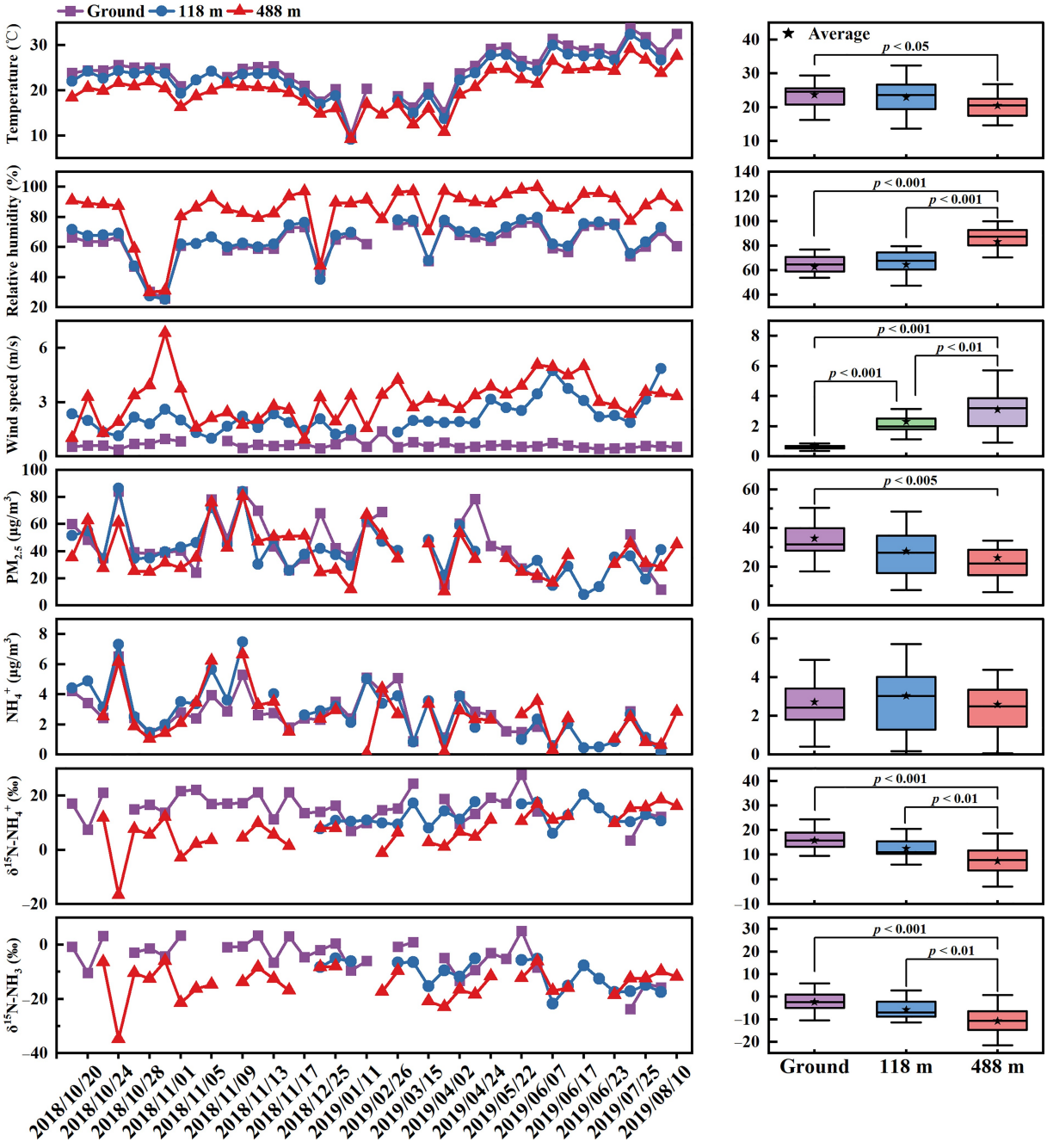

Fig. 1 The left panel displays the time series of temperature (°C), relative humidity (%), wind speed (m/s), $PM_{2.5}$ concentration (μg/m^3), NH_4^+ concentration (μg/m^3), $\delta^{15}N\text{-}NH_4^+$ (‰), and the initial $\delta^{15}N\text{-}NH_3$ (‰). The right panel presents the average values at different heights, highlighting statistically significant differences.

emissions of vehicle exhaust, biomass burning, coal combustion, NH_3 slip, livestock, fertilizer application, and waste (Huang et al., 2021). Therefore, it is essential to revisit the $\delta^{15}N\text{-}NH_3$ endmembers of these sources to improve the accuracy of NH_3 source apportionment based on ^{15}N measurements. Since a large ^{15}N diffusion fractionation occurs during the process of passive sampling for NH_3 (Pan et al., 2020), only $\delta^{15}N\text{-}NH_3$ values of the sources using the active sampling technique were considered in this study.

In total, more than 300 $\delta^{15}N\text{-}NH_3$ values for 7 sources were obtained based on 13 studies (Table S3). Obviously, the $\delta^{15}N\text{-}NH_3$ values in the combustion-related sources were significantly higher than those in

Table 1 Measure $\delta^{15}N\text{-}NH_4^+$ values (‰) at three heights of the Canton Tower

Season	Sampling time	$\delta^{15}N\text{-}NH_4^+$			Season	Sampling time	$\delta^{15}N\text{-}NH_4^+$		
		Ground	118 m	488 m			Ground	118 m	488 m
Autumn	2018/10/18	17	/	/	Winter	2019/1/19	15	9.9	−1.1
Autumn	2018/10/20	7.5	/	/	Winter	2019/2/26	15	9.4	6.4
Autumn	2018/10/22	21	/	12	Spring	2019/3/6	25	17	/
Autumn	2018/10/24		/	−17	Spring	2019/3/15	/	8.0	2.8
Autumn	2018/10/26	15	/	7.8	Spring	2019/3/23	19	14	1.2
Autumn	2018/10/28	17	/	5.6	Spring	2019/4/2	9.6	11	6.7
Autumn	2018/10/30	14	/	12	Spring	2019/4/17	13	18	4.8
Autumn	2018/11/1	22	/	−2.9	Spring	2019/4/24	19	/	11.2
Autumn	2018/11/3	22	/	2.2	Spring	2019/5/14	17	/	/
Autumn	2018/11/5	17	/	3.6	Spring	2019/5/22	28	17	11
Autumn	2018/11/7	17	/	/	Spring	2019/5/29	14	18	17
Autumn	2018/11/9	17	/	4.5	Summer	2019/6/7	/	6.1	11
Autumn	2018/11/11	21	/	9.9	Summer	2019/6/15	/	13	13
Autumn	2018/11/13	11	/	5.6	Summer	2019/6/17	/	21	/
Autumn	2018/11/15	21	/	1.5	Summer	2019/6/18	/	15	/
Autumn	2018/11/17	14	/	/	Summer	2019/6/23	/	11	9.9
Winter	2018/12/17	14	7.8	8.0	Summer	2019/7/16	3.5	10	15
Winter	2018/12/25	16	11	8.1	Summer	2019/7/25	13	13	16
Winter	2019/1/2	7.1	11	/	Summer	2019/8/2	12	11	19
Winter	2019/1/11	9.9	11.0	/	Summer	2019/8/10	/	/	16

Notes: The data for autumn were obtained from the study by Chen et al. (2022). "/" indicates that the data are missing.

volatilization sources. Also, all $\delta^{15}N\text{-}NH_3$ values among sources were significantly different ($p < 0.05$), except for the values between fertilizer application and livestock ($p > 0.05$) (Fig. 2), suggesting that it is preferable to combine fertilizer application and livestock into a single agricultural source. Therefore, the $\delta^{15}N\text{-}NH_3$ endmembers were categorized as follows (Table S4): agriculture (−25‰ ± 6.1‰), waste (−33‰ ± 5.0‰), coal combustion (−18‰ ± 6.5‰), biomass burning (−11‰ ± 6.4‰), NH_3 slip (−2.8‰ ± 7.8‰), and vehicle exhaust (3.4‰ ± 5.0‰). Furthermore, the six primary ammonia sources were divided into two distinct types: combustion-related sources (−7.1 ‰ ± 3.2 ‰) and volatilization sources (−28 ‰ ± 3.2 ‰). Combustion-related sources include vehicle exhaust, NH_3 slip, and coal combustion, while volatilization sources comprise agriculture and waste.

3.4 Source apportionment of NH_3 in different heights in the PRD region

In this study, the average of the initial $\delta^{15}N\text{-}NH_3$ values at the ground site, 118 m, and 488 m were −2.3 ‰ ± 5.2 ‰, −5.8 ‰ ± 3.9 ‰, and −11 ‰ ± 7.3 ‰, respectively. The average value of the initial $\delta^{15}N\text{-}NH_3$ at the ground level was 2.5 and 4.7 times higher than those at 118 m and 488 m, indicating that NH_3 at the ground level is more influenced by $\delta^{15}N$-rich emission sources than by those in the higher atmosphere. Figure 3 illustrates the source apportionment of atmospheric NH_3 using the estimated initial $\delta^{15}N\text{-}NH_3$ values based on two assumptions. Whether NH_3 emissions are assumed to originate from six sources (vehicle, NH_3 slip, biomass burning, coal combustion, agriculture, waste) or two sources (combustion and volatilization), the results consistently indicate that combustion sources are significant contributors to NH_3 in this megacity of the PRD region. In the case of six sources, the largest source of NH_3 at the ground site was vehicle (29%), followed by NH_3 slip (25%), biomass burning (16%), coal combustion (12%), agriculture (10%), and waste (8%), meaning that the contributions of combustion sources and volatilization sources were 82% and 18%, respectively. This result is very close to the scenario where only two sources are considered in the SIAR model, which showed that the

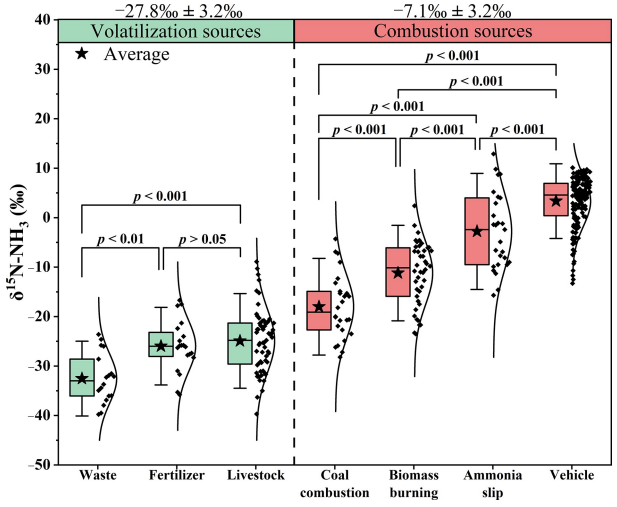

Fig. 2 Endmembers of δ^{15}N-NH_3 from different emission sources obtained using active sampling techniques. Data were sourced from the references of Bokhoven and Theeuwen (1966); Feryer (1978); Heaton (1987); Smirnoff et al. (2012); David Felix et al. (2013); Berner and David Felix (2020); Bhattarai et al. (2020); Shao et al. (2020); Walters et al. (2020); Song et al. (2021); Chang et al. (2022); Li et al. (2023); Wu et al. (2024).

contribution of combustion sources to NH_3 at the ground site was 87% with the remaining 13% from volatilization sources (Fig. 3). This strong agreement between the two scenarios suggests that the dataset of the δ^{15}N-NH_3 endmembers in sources is reliable for source apportionment of NH_3. It is important to note that the influence of volatilization sources on NH_3 becomes more pronounced with increasing height, as confirmed by observations in North China (Zhang et al., 2020), mainly due to the limited influence of local combustion-related emissions at higher altitudes.

Different seasonal characteristics of NH_3 source apportionments were found at different heights (Fig. 4). At the ground site, which is easily influenced by the local sources, the largest NH_3 source is vehicle with a contribution of 32% in autumn, followed by NH_3 slip (28%), biomass burning (15%), coal combustion (11%), agriculture (8%), and waste (6%). This meant that the volatilization sources accounted for only 14% during this season. Similar source contribution profiles were also observed during winter and spring at the ground site. However, in summer, the volatilization sources contributed as much as 40% due to the high temperatures during this season, which may strongly enhance the emission of NH_3 from these types of sources. The seasonal variation of the NH_3 source contribution profile at 488 m is notably different from that at the ground site. The contributions of all sources exhibit a relatively stable level throughout the year at an altitude of 488 m, indicating that NH_4^+ particles at this height are less influenced by direct NH_3 emissions from various sources and can serve as a more reliable receptor site for the PRD region. Nevertheless, the contribution of volatilization sources (27%–35%) to NH_3 at 488 m remains considerably lower than that of combustion sources (65%–73%) throughout all seasons. Taken together, all the seasonal and vertical variations in the source apportionment of NH_3 in this study strongly suggest that combustion activity is the dominant source of NH_3 in the PRD region.

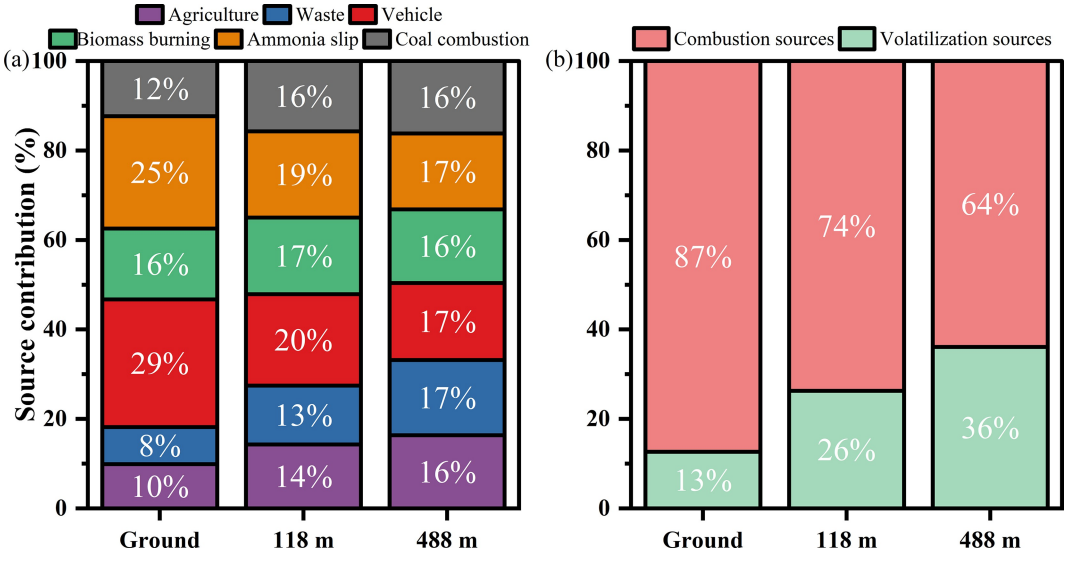

Fig. 3 Contributions of different sources to NH_3 based on the SIAR model under the scenarios of (a) six sources and (b) two sources.

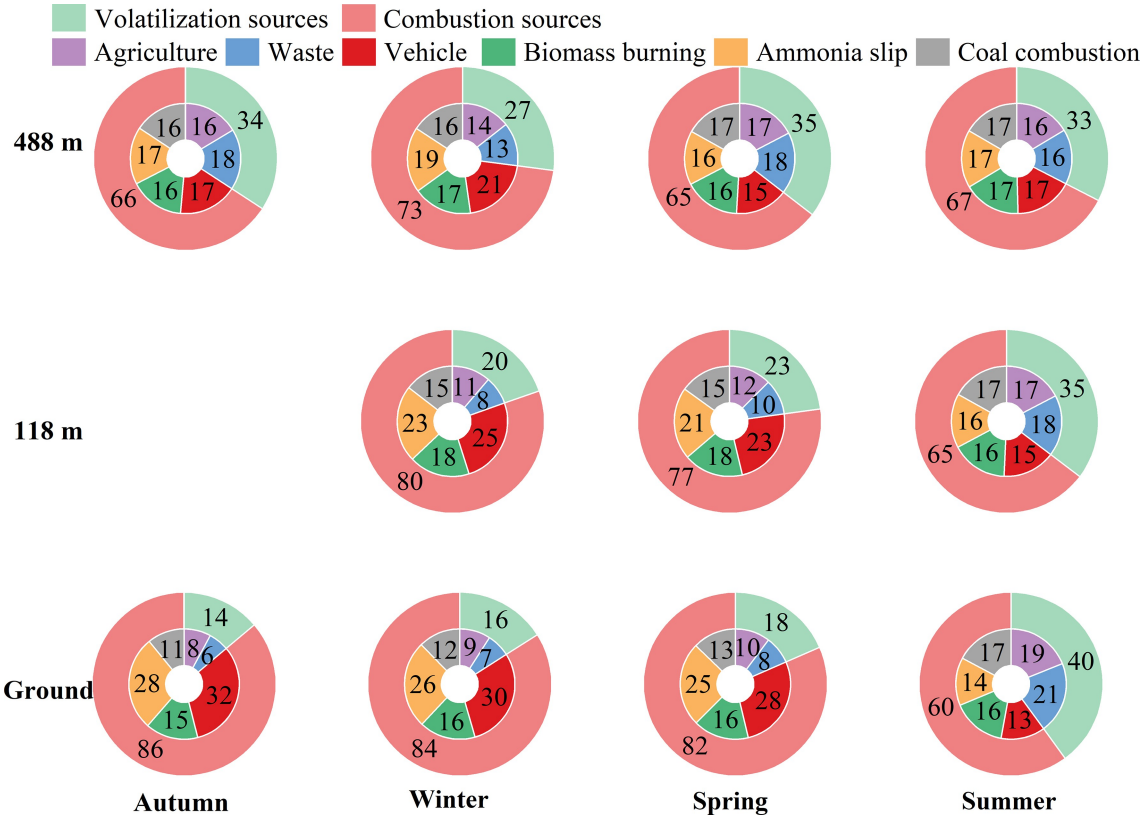

Fig. 4 Seasonal contributions of different sources to NH_3 at ground site, 118 m, and 488 m.

3.5 Uncertainty analysis of *f* on the results of the source apportionment using SIAR

In this study, the *f* value was obtained from the previous research conducted in the PRD region (Yue et al., 2015), which is comparable to those in other cities in China (Table S5). A prior study found that the NH_3 concentrations did not vary significantly across different altitudes in urban areas of China (Zhang et al., 2018). The NH_4^+ concentrations in this study also showed no significant variation with altitude and aligned with the vertical distribution patterns of NH_3 in urban areas of China. In addition, the NH_4^+ concentrations were insignificantly correlated with temperature or humidity ($p > 0.05$). These findings indicate that the gas-to-particle conversion of atmospheric NH_3 did not vary significantly across different altitudes in Guangzhou during the sampling period. Therefore, we used the *f* value from the near-ground levels at all altitudes, consistent with previous studies conducted at the 325 m meteorological tower in Beijing (Wu et al., 2019; Zhang et al., 2020; Wu et al., 2024).

To assess the impact of the *f* value on the results of the source apportionment of NH_3, a detailed sensitivity analysis of the *f* value in the SIAR model was performed. When the *f* values were adjusted by decreasing or increasing them by 10%, 20%, 30%,40%, and 50%, the average uncertainties for the NH_3 source apportionments from agricultural, waste, vehicle exhaust, biomass burning, NH_3 slip, and coal combustion were 18%, 26%, 18%, 3.6%, 18%, and 10%, respectively. The average uncertainties in the NH_3 source apportionment at ground, 118 m, and 488 m were 20%, 14%, and 13%, respectively. Figure 5 demonstrates that combustion sources were the dominant contributors to NH_3 at all heights, and their contribution decreased with increasing altitude regardless of how the *f* values varied within the range of sensitivity analyses.

4 Conclusions

We measured NH_4^+ concentrations and their $\delta^{15}N$ signatures at three atmospheric observatories (ground, 118 m, 488 m) at the Canton Tower in Guangzhou, China. The average concentrations of NH_4^+ were 2.7 ± 1.4 μg/m^3 at the ground site, 3.0 ± 1.8 μg/m^3 at 118 m, and 2.6 ± 1.7 μg/m^3 at 488 m. A strong positive

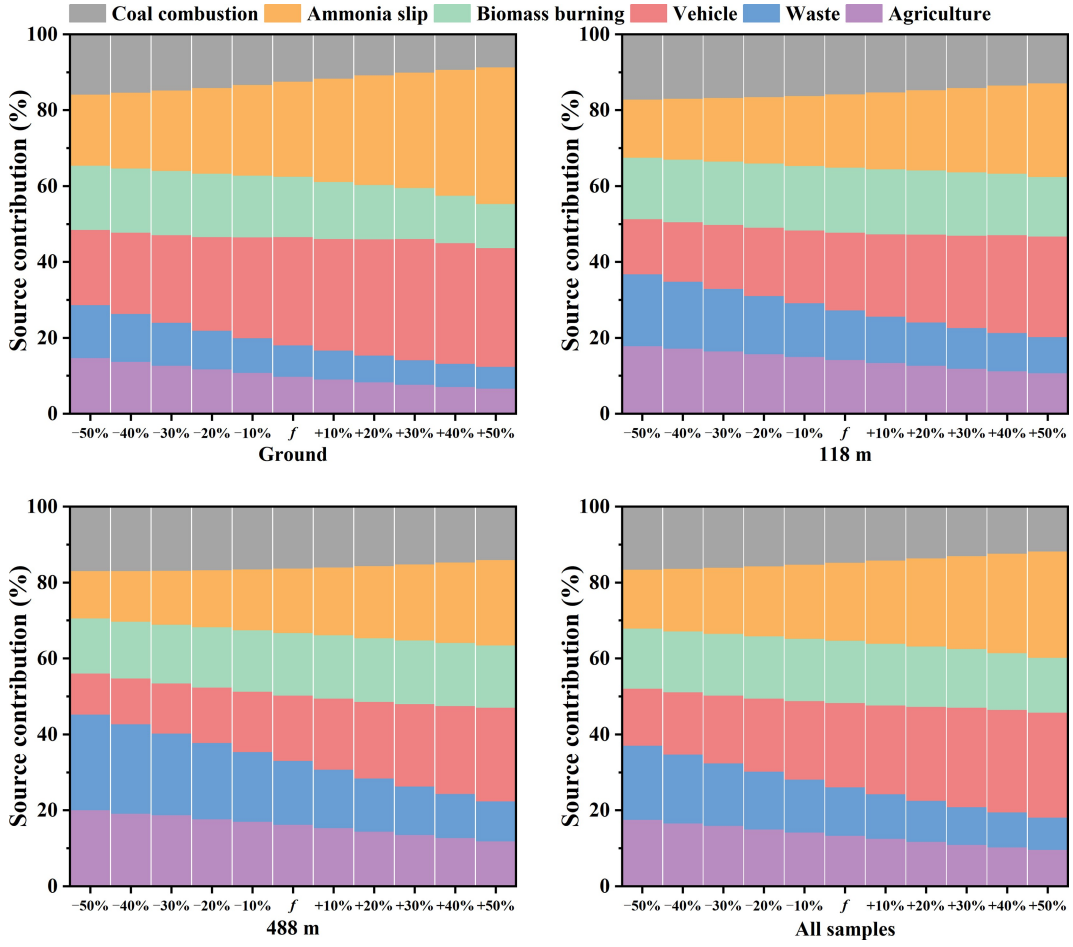

Fig. 5 Sensitivity analysis of the *f* value on the results of the NH_3 source apportionment in the SIAR model.

correlation was observed between NH_4^+ and $PM_{2.5}$ concentrations at all heights ($p < 0.001$), suggesting that NH_4^+ is a key component driving $PM_{2.5}$ formation in the PRD region. Significant differences were found in $\delta^{15}N\text{-}NH_4^+$ signatures among the heights ($p < 0.01$), with values of 16‰ ± 5.2‰ at the ground site, 12‰ ± 3.8 ‰ at 118 m, and 7.4 ‰ ± 7.1 ‰ at 488 m. Additionally, we calculated the initial $\delta^{15}N\text{-}NH_3$ values, and the SIAR model revealed that the contributions from different sources varied with height. On average, the contributions from agriculture, waste, vehicle, biomass burning, NH_3 slip, and coal combustion at the ground site were 9.9% ± 4.4%, 8.3% ± 5.5%, 29% ± 8.0%, 16% ± 2.2%, 25% ± 6.0%, and 12% ± 3.4%, respectively. By contrast, the corresponding contributions were 14% ± 3.6%, 13% ± 5.7%, 20% ± 5.9%, 17% ± 0.84%, 19% ± 4.0%, and 16% ± 1.4% at 118 m, and 16% ± 3.5%, 17% ± 8.1%, 17% ± 5.7%, 16% ± 2.2%, 17% ± 4.0%, and 16% ± 1.6% at 488 m, respectively. Overall, our findings suggest that combustion sources are the predominant contributors to the atmospheric NH_4^+ loading in this highly urbanized region of China, rather than volatilization sources. These insights should be seriously considered in future NH_3 emission reduction strategies and $PM_{2.5}$ pollution mitigation efforts.

Conflict of Interests The authors declare that they have no known competing financial interests or personal relationships that could have appeared to influence the work reported in this manuscript.

Acknowledgements This study was supported by the National Natural Science Foundation of China (No. 42230602), the National Key Research and Development Program of China (No. 2022YFC3700602), and the Guang Dong Basic and Applied Basic Research Foundation (China) (No. 2024B1515040026).

Electronic Supplementary Material Supplementary material is available in the online version of this article at https://doi.org/10.1007/s11783-025-1997-4 and is accessible for authorized users.

References

Berner A H, David Felix J (2020). Investigating ammonia emissions

in a coastal urban airshed using stable isotope techniques. Science of the Total Environment, 707: 134952

Bhattarai N, Wang S, Xu Q, Dong Z, Chang X, Jiang Y, Zheng H (2020). Sources of gaseous NH_3 in urban Beijing from parallel sampling of NH_3 and NH_4^+, their nitrogen isotope measurement and modeling. Science of the Total Environment, 747: 141361

Bokhoven C, Theeuwen H J (1966). Determination of the abundance of carbon and nitrogen isotopes in Dutch coals and natural gas. Nature, 211(5052): 927–929

Chang Y, Cheng K, Kuang Y, Hu Q, Gao Y, Huang R J, Huang C, Walters W W, Lehmann M F (2022). Isotopic variability of ammonia (δ^{15}N-NH_3) slipped from heavy-duty vehicles under real-world conditions. Environmental Science & Technology Letters, 9(9): 726–732

Chang Y, Zhang Y L, Kawichai S, Wang Q, Van Damme M, Clarisse L, Prapamontol T, Lehmann M F (2021). Convergent evidence for the pervasive but limited contribution of biomass burning to atmospheric ammonia in peninsular Southeast Asia. Atmospheric Chemistry and Physics, 21(9): 7187–7198

Chen Z, Pei C, Liu J, Zhang X, Ding P, Dang L, Zong Z, Jiang F, Wu L, Sun X, Zhou S, Zhang Y, Zhang Z, Zheng J, Tian C, Li J, Zhang G (2022). Non-agricultural source dominates the ammonium aerosol in the largest city of South China based on the vertical δ^{15}N measurements. Science of the Total Environment, 848: 157750

David Felix J, Elliott E M, Gish T J, Mcconnell L L, Shaw S L (2013). Characterizing the isotopic composition of atmospheric ammonia emission sources using passive samplers and a combined oxidation-bacterial denitrifier approach. Rapid Communications in Mass Spectrometry, 27(20): 2239–2246

EEA (2023). European Union Emission Inventory Report 1990–2022—Under the UNECE Convention on Long-range Transboundary Air Pollution (Air Convention). Copenhagen, Denmark: EEA

Farren N J, Davison J, Rose R A, Wagner R L, Carslaw D C (2020). Underestimated ammonia emissions from road vehicles. Environmental Science & Technology, 54(24): 15689–15697

Felix J D, Berner A, Wetherbee G A, Murphy S F, Heindel R C (2023). Nitrogen isotopes indicate vehicle emissions and biomass burning dominate ambient ammonia across Colorado's Front Range urban corridor. Environmental Pollution, 316: 120537

Feng S, Xu W, Cheng M, Ma Y, Wu L, Kang J, Wang K, Tang A, Collett J L Jr, Fang Y, et al. (2022). Overlooked nonagricultural and wintertime agricultural NH_3 emissions in Quzhou County, North China Plain: evidence from ^{15}N-stable isotopes. Environmental Science & Technology Letters, 9(2): 127–133

Feng X, Chen Y, Du H, Feng Y, Mu Y, Chen J (2023). Biomass burning is a non-negligible source for ammonium during winter haze episodes in rural North China: evidence from high time resolution ^{15}N-stable isotope. Journal of Geophysical Research: Atmospheres, 128(3): e2022JD038012

Feryer H D (1978). Seasonal trends of NH_4^+ and NO_3^- nitrogen isotope composition in rain collected at Jiilich, Germany. Tellus, 30(1): 83–92

Gu B, Zhang L, Dingenen R V, Vieno M, Grinsven H J V, Zhang X, Zhang S, Chen Y, Wang S, Ren C, et al. (2021). Abating ammonia is more cost-effective than nitrogen oxides for mitigating $PM_{2.5}$ air pollution. Science, 374(6568): 758–762

Heaton T H E (1987). ^{15}N/^{14}N ratios of nitrate and ammonium in rain at Pretoria, South Africa. Atmospheric Environment, 21(4): 843–852

Huang Z, Zhong Z, Sha Q, Xu Y, Zhang Z, Wu L, Wang Y, Zhang L, Cui X, Tang M, et al. (2021). An updated model-ready emission inventory for Guangdong Province by incorporating big data and mapping onto multiple chemical mechanisms. Science of the Total Environment, 769: 144535

Jiang F, Liu J, Cheng Z, Ding P, Xu Y, Zong Z, Zhu S, Zhou S, Yan C, Zhang Z, et al. (2022). Dual-carbon isotope constraints on source apportionment of black carbon in the megacity Guangzhou of the Pearl River Delta region, China for 2018 autumn season. Environmental Pollution, 294: 118638

Jiang F, Liu J, Cheng Z, Ding P, Zhu S, Yuan X, Chen W, Zhang Z, Zong Z, Tian C, et al. (2023). Quantitative evaluation for the sources and aging processes of organic aerosols in urban Guangzhou: insights from a comprehensive method of dual-carbon isotopes and macro tracers. Science of the Total Environment, 888: 164182

Kawashima H, Ono S (2019). Nitrogen isotope fractionation from ammonia gas to ammonium in particulate ammonium chloride. Environmental Science & Technology, 53(18): 10629–10635

Kawashima H, Yoshida O, Suto N (2023). Long-term source apportionment of ammonium in $PM_{2.5}$ at a suburban and a rural site using stable nitrogen isotopes. Environmental Science & Technology, 57(3): 1268–1277

Li B, Chen L, Shen W, Jin J, Wang T, Wang P, Yang Y, Liao H (2021). Improved gridded ammonia emission inventory in China. Atmospheric Chemistry and Physics, 21(20): 15883–15900

Li L, Lollar B S, Li H, Wortmann U G, Lacrampe-Couloume G (2012). Ammonium stability and nitrogen isotope fractionations for NH_4^+-NH_3(aq)-NH_3(gas) systems at 20–70 °C and pH of 2–13: applications to habitability and nitrogen cycling in low-temperature hydrothermal systems. Geochimica et Cosmochimica Acta, 84: 280–296

Li M, Liu H, Geng G, Hong C, Liu F, Song Y, Tong D, Zheng B, Cui H, Man H, et al. (2017a). Anthropogenic emission inventories in China: a review. National Science Review, 4(6): 834–866

Li Y, Liu J, George C, Herrmann H, Gu M, Yang M, Wang Y, Mellouki A, Pan Y, Felix J D, et al. (2023). Apportioning atmospheric ammonia sources across spatial and seasonal scales by their isotopic fingerprint. Environmental Science & Technology, 57(43): 16424–16434

Li Y, Thompson T M, Van Damme M, Chen X, Benedict K B, Shao Y, Day D, Boris A, Sullivan A P, Ham J, et al. (2017b). Temporal and spatial variability of ammonia in urban and agricultural regions of northern Colorado, United States.

Atmospheric Chemistry and Physics, 17(10): 6197–6213

Liu D, Fang Y, Tu Y, Pan Y (2014). Chemical method for nitrogen isotopic analysis of ammonium at natural abundance. Analytical Chemistry, 86(8): 3787–3792

Liu J, Ding P, Zong Z, Li J, Tian C, Chen W, Chang M, Salazar G, Shen C, Cheng Z, et al. (2018). Evidence of rural and suburban sources of urban haze formation in China: a case study from the Pearl River Delta region. Journal of Geophysical Research. Atmospheres, 123(9): 4712–4726

Nirmalkar J, Jung J, Han S, Dong Z, Xu Z, Fu P, Pavulari C M (2023). Chemistry of $PM_{2.5}$ in haze events in two East Asian cities during winter–spring 2019. Atmospheric Environment, 293: 119457

Pan Y, Gu M, Song L, Tian S, Wu D, Walters W W, Yu X, Lü X, Ni X, Wang Y, et al. (2020). Systematic low bias of passive samplers in characterizing nitrogen isotopic composition of atmospheric ammonia. Atmospheric Research, 243: 105018

Pan Y, Tian S, Liu D, Fang Y, Zhu X, Zhang Q, Zheng B, Michalski G, Wang Y (2016). Fossil fuel combustion-related emissions dominate atmospheric ammonia sources during severe haze episodes: evidence from ^{15}N-stable isotope in size-resolved aerosol ammonium. Environmental Science & Technology, 50(15): 8049–8056

Parnell A C, Inger R, Bearhop S, Jackson A L (2010). Source partitioning using stable isotopes: coping with too much variation. PLoS One, 5(3): e9672

Sahoo P, Sahu S K, Mangaraj P, Mishra A, Beig G, Gunthe S S (2024). Reporting of gridded ammonia emission and assessment of hotspots across India: a comprehensive study of 24 anthropogenic sources. Journal of Hazardous Materials, 479: 135557

Shao S, Zhang Y, Chang Y, Cao F, Lin Y, Mozaffar A, Hong Y (2020). Online characterization of a large but overlooked human excreta source of ammonia in China's urban atmosphere. Atmospheric Environment, 230: 117459

Smirnoff A, Savard M M, Vet R, Simard M C (2012). Nitrogen and triple oxygen isotopes in near‐road air samples using chemical conversion and thermal decomposition. Rapid Communications in Mass Spectrometry, 26(23): 2791–2804

Song L, Walters W W, Pan Y, Li Z, Gu M, Duan Y, Lü X, Fang Y (2021). ^{15}N natural abundance of vehicular exhaust ammonia, quantified by active sampling techniques. Atmospheric Environment, 255: 118430

U.S.EPA (2023). EPA's 2020 National Emissions Inventory and Trends Report. Washington, DC: U.S.EPA

Urey H C (1947). The thermodynamic properties of isotopic substances. Journal of the Chemical Society (Resumed), 1947(5): 562–581

Van Damme M, Clarisse L, Whitburn S, Hadji-Lazaro J, Hurtmans D, Clerbaux C, Coheur P F (2018). Industrial and agricultural ammonia point sources exposed. Nature, 564(7734): 99–103

Vo T, Christiansen A E (2024). Impact of recent agricultural ammonia increases on fine particulate matter burden over the Midwestern United States. ACS Earth & Space Chemistry, 8(11): 2209–2217

Walters W W, Chai J, Hastings M G (2019). Theoretical phase resolved ammonia–ammonium nitrogen equilibrium isotope exchange fractionations: applications for tracking atmospheric ammonia gas-to-particle conversion. ACS Earth & Space Chemistry, 3(1): 79–89

Walters W W, Karod M, Willcocks E, Baek B H, Blum D E, Hastings M G (2022). Quantifying the importance of vehicle ammonia emissions in an urban area of northeastern USA utilizing nitrogen isotopes. Atmospheric Chemistry and Physics, 22(20): 13431–13448

Walters W W, Song L, Chai J, Fang Y, Colombi N, Hastings M G (2020). Characterizing the spatiotemporal nitrogen stable isotopic composition of ammonia in vehicle plumes. Atmospheric Chemistry and Physics Discussion, 20(19): 11551–11567

Wang W, Gao Y, Shao L, Fan C, Li X, Li Y, Liu M, Zhou X (2023a). Chemical compositions and possible transportation of $PM_{2.5}$ during two haze periods in a coastal city of the North China Plain. Geological Journal, 58(12): 4417–4427

Wang Y, Liu J, Jiang F, Chen Z, Wu L, Zhou S, Pei C, Kuang Y, Cao F, Zhang Y, et al. (2023b). Vertical measurements of stable nitrogen and oxygen isotope composition of fine particulate nitrate aerosol in Guangzhou city: source apportionment and oxidation pathway. Science of the Total Environment, 865: 161239

Weagle C L, Snider G, Li C, Van Donkelaar A, Philip S, Bissonnette P, Burke J, Jackson J, Latimer R, Stone E, et al. (2018). Global sources of fine particulate matter: interpretation of $PM_{2.5}$ chemical composition observed by SPARTAN using a global chemical transport model. Environmental Science & Technology, 52(20): 11670–11681

Wei Y, Tian X, Huang J, Wang Z, Huang B, Liu J, Gao J, Liang D, Yu H, Feng Y, et al. (2023). New insights into the formation of ammonium nitrate from a physical and chemical level perspective. Frontiers of Environmental Science & Engineering, 17(11): 137

Wu L, Ren H, Wang P, Chen J, Fang Y, Hu W, Ren L, Deng J, Song Y, Li J, et al. (2019). Aerosol ammonium in the urban boundary layer in Beijing: insights from nitrogen isotope ratios and simulations in summer 2015. Environmental Science & Technology Letters, 6(7): 389–395

Wu L, Wang P, Zhang Q, Ren H, Shi Z, Hu W, Chen J, Xie Q, Li L, Yue S, et al. (2024). Dominant contribution of combustion-related ammonium during haze pollution in Beijing. Science Bulletin, 69(7): 978–987

Xiao H W, Wu J F, Luo L, Liu C, Xie Y J, Xiao H (2020). Enhanced biomass burning as a source of aerosol ammonium over cities in central China in autumn. Environmental Pollution, 266: 115278

Xu W, Zhao Y, Wen Z, Chang Y, Pan Y, Sun Y, Ma X, Sha Z, Li Z, Kang J J S B, et al. (2022). Increasing importance of ammonia emission abatement in $PM_{2.5}$ pollution control. Science Bulletin, 67(17): 1745–1749

Yue D, Zhong L, Zhang T, Shen J, Zhou Y, Zeng L, Dong H, Ye S (2015). Pollution properties of water-soluble secondary inorganic ions in atmospheric $PM_{2.5}$ in the Pearl River Delta Region. Aerosol and Air Quality Research, 15(5): 1737–1747

Zhang Y, Benedict K B, Tang A, Sun Y, Fang Y, Liu X (2020). Persistent nonagricultural and periodic agricultural emissions dominate sources of ammonia in urban Beijing: evidence from ^{15}N stable isotope in vertical profiles. Environmental Science & Technology, 54(1): 102–109

Zhang Y, Ma X, Tang A, Fang Y, Misselbrook T, Liu X (2023). Source apportionment of atmospheric ammonia at 16 sites in China using a Bayesian isotope mixing model based on $\delta^{15}N$-NH_x signatures. Environmental Science & Technology, 57(16): 6599–6608

Zhang Y, Tang A, Wang D, Wang Q, Benedict K, Zhang L, Liu D, Li Y, Collett J L Jr, Sun Y, et al. (2018). The vertical variability of ammonia in urban Beijing, China. Atmospheric Chemistry and Physics, 18(22): 16385–16398

Zheng M, Wang Y, Yuan L, Chen N, Kong S (2022). Ambient observations indicating an increasing effectiveness of ammonia control in wintertime $PM_{2.5}$ reduction in Central China. Science of the Total Environment, 824: 153708